



Ionic conductivity of the LiOH-Li₂SO₄ system and fabrication of all-solid-state lithium batteries

Reona Miyazaki¹ · En Yagi² · Satoshi Ozaki² · Yusaku Suto² · Harunobu Onishi² · Yosuke Sato² · Toshihiro Yoshida² · Yuji Katsuda²

Received: 8 August 2023 / Revised: 24 August 2023 / Accepted: 25 August 2023 / Published online: 6 September 2023
© The Author(s), under exclusive licence to Springer-Verlag GmbH Germany, part of Springer Nature 2023

Abstract

The solid electrolytes with a low melting temperature are promising for the all-solid-state lithium batteries because such electrolytes enable the battery fabrication without high-temperature sintering (for example, ~1000 °C for oxide materials). In this study, a series of LiOH-Li₂SO₄ systems with different LiOH/Li₂SO₄ ratios is fabricated by melting LiOH and Li₂SO₄ at 430 °C, and their ion conduction properties are investigated. The stoichiometric compounds are obtained in 2.2LiOH·Li₂SO₄ without segregation of LiOH and Li₂SO₄, which is rather different from the previously known composition (3LiOH·Li₂SO₄). The deviation from this LiOH/Li₂SO₄ fraction results in a segregation of LiOH or Li₂SO₄. The conductivities of 2.2LiOH·Li₂SO₄ with 5 mol% of Li₃BO₃ are 1.9×10^{-6} and 6.0×10^{-3} S/cm at 25 and 150 °C, respectively. The all-solid-state batteries are fabricated by hot pressing the solid electrolyte with Li(Ni_{0.3}Co_{0.6}Mn_{0.1})O₂ (cathode) and graphite (anode) at 250 °C under 150 MPa. The contacts of the solid electrolyte with Li(Ni_{0.3}Co_{0.6}Mn_{0.1})O₂ and graphite are intimate, and the by-products are not found at the interphase. The discharge capacities of 80 mAh/g are obtained for 100 cycles at 150 °C when the charging voltage is restricted to 3.95 V. The results of cyclic voltammetry measurement indicate the reductive decomposition of the solid electrolyte at 2.3 and 1.6 V. These reduction currents are decreased with cycling, suggesting the passivation of the anode interphase. On the other hand, the oxidation current is observed above 3.6 V which is not terminated during voltage cycling. In the battery fabrication process, high-temperature sintering is not necessary, and the dense contacts with electrode materials can be made by hot pressing at 250 °C. Furthermore, the batteries are constructed in a dry room where the dew point is maintained at -40 °C. The present results suggest the potential of the LiOH-Li₂SO₄ as the solid electrolyte for all-solid-state lithium batteries.

Keywords Solid electrolyte · LiOH-Li₂SO₄ · All-solid-state lithium battery

Introduction

Solid electrolytes in which Li⁺ ions migrate in their crystal lattices are crucial for the realization of all-solid-state lithium-ion batteries (LIBs). Because the ceramic solid electrolytes are used, all-solid-state LIBs fundamentally avoid the battery explosion, which is a clear contrast to the conventional LIBs with flammable organic liquid electrolytes.

The high energy density is also the promising feature of all-solid-state LIBs because high-capacity cathode materials can be used [1, 2].

Not only the high Li⁺ conductivity but also the intimate contact between the cathode (anode) and the solid electrolyte is also essential for the facile electrochemical reaction at the interphases. The construction of such a dense interphase has been less concerned for the conventional LIBs because the liquid electrolytes spontaneously infiltrate and form the homogeneous contact with electrode materials. However, for the case of the oxide solid electrolytes, the construction of the intimate interphase with electrodes is challenging. High-temperature sintering is necessary for the densification of the interphase while the secondary phase presents at the interphase as the results of the chemical reaction between the solid electrolyte and the active material [3]. Hence, the

✉ Reona Miyazaki
miyazaki.reona@nitech.ac.jp

¹ Department of Physical Science and Engineering, Graduate School of Engineering, Nagoya Institute of Technology, Nagoya 466-8555, Japan

² NGK INSULATORS, LTD, 2-56 Suda-Cho, Mizuho, Nagoya 467-8530, Japan

solid electrolytes which can form the intimate contact with electrodes without sintering are highly desirable for the high-performance batteries.

The dense pellets of the sulfide solid electrolyte were obtained only by uniaxial pressing without sintering, which is the clear contrast to the oxide electrolytes [4]. The flexible and soft features are also known for hydrides, halides, and oxyhalides solid electrolytes [4–7]. For example, all-solid-state LIBs using LiBH_4 have been constructed by uniaxial pressing at room temperature, resulting in the high charge–discharge performances [5, 8]. Oxyhalide with an anti-perovskite structure, Li_2OHBr , exhibits a high deformable nature; the dense pellet with relative density of 95% has been obtained by pressing without sintering [7, 9]. Such a highly deformable electrolyte is of great advantage for large-scale production of batteries because the heating process is not included in the battery fabrication process. The low melting temperature is also the key for the promising solid electrolytes because the high-temperature sintering is not needed for constructing the dense interphase, which avoids the side reaction with the active materials. High deformability can also be expected for the solid electrolytes with low melting temperature; high-density pellets are obtained by uniaxial pressing at room temperature [10–12].

Biefeld and Johnson have reported the stoichiometric compound of $3\text{LiOH}\cdot\text{Li}_2\text{SO}_4$ in the $\text{LiOH}\text{--}\text{Li}_2\text{SO}_4$ pseudobinary system, whose melting temperature was approximately $400\text{ }^\circ\text{C}$ [13]. The moderately low melting temperature of this compound indicates the high pressing ability and formation of the intimate contact with electrode materials without sintering. Deshpande et al. has reported the compositional dependence of the conductivities in the $\text{LiOH}\text{--}\text{Li}_2\text{SO}_4$ system in which the maximum conductivity is of the order of 10^{-2} S/cm at 558 K for 20 mol% of Li_2SO_4 [14]. Despite its high conductivity and low melting temperature, the $\text{LiOH}\text{--}\text{Li}_2\text{SO}_4$ system has not been focused as the battery materials after the report of Singh et al. in 1988 [15]. Recently, $\text{LiOH}\text{--}\text{Li}_2\text{SO}_4$ has been used as the molten salt for the preparation of the single crystal of Ni-rich cathodes [16–19]. However, to the best of the authors' knowledge, the charge–discharge performances of the battery with $\text{LiOH}\text{--}\text{Li}_2\text{SO}_4$ solid electrolyte have not been reported so far.

In the present study, $\text{LiOH}\text{--}\text{Li}_2\text{SO}_4$ systems with the different $\text{LiOH}/\text{Li}_2\text{SO}_4$ ratios were fabricated by melting, and the specific composition in which the single phase of the line compound is obtained was determined. The compositional dependence of the conductivity was investigated. For the enhancement of the conductivity, the trace amount of Li_3BO_3 was added, whose compositional dependence was also investigated. All-solid-state LIBs of graphite (anode) and $\text{Li}(\text{Ni}_{0.3}\text{Co}_{0.6}\text{Mn}_{0.1})\text{O}_2$ (cathode) were constructed using $2.2\text{LiOH}\cdot\text{Li}_2\text{SO}_4$ with 5 mol% of Li_3BO_3 by hot pressing, and these charge–discharge performances were

characterized. The electrochemical stabilities were also investigated. The charge–discharge performances and electrochemical stability of $2.2\text{LiOH}\cdot\text{Li}_2\text{SO}_4$ with 5 mol% of Li_3BO_3 were discussed in conjunction with the variation of the microstructure of electrode interphase.

Experimental

Unless otherwise noted, all experimental procedures mentioned below were conducted in an Ar-filled glove box where the oxygen concentration and dew point were kept at several ppm and $-80\text{ }^\circ\text{C}$, respectively.

Materials

LiOH (Sigma-Aldrich) and Li_2SO_4 (Sigma-Aldrich) were mixed and ground in a given molar ratio using an agate pestle. The powder mixture was put in an alumina crucible and melted at $430\text{ }^\circ\text{C}$ for 2 h in the glove box. The melt was quenched by casting the melt onto the Al block. Li_3BO_3 (Toshiba Manufacturing Co., Ltd.) was mixed with $\text{LiOH}\text{--}\text{Li}_2\text{SO}_4$ in a similar manner.

XRD measurement

The crystal structure of a series of $\text{LiOH}\text{--}\text{Li}_2\text{SO}_4$ systems was investigated by XRD with $\text{Cu}\text{--}\text{K}\alpha$ radiation. To avoid the air exposure, the powder samples were sealed with Kapton[®] tape during the measurements. Si powder was mixed in the sample and used as an internal standard of the peak positions.

SEM observation

The microstructures of the cathode and anode interphases were observed by SEM (HITACHI, S3400). The fracture of the pellet was polished by a focused ion beam (FIB) equipped in SEM, and the cross-section was observed. The samples were mounted in the air-tight holder and SEM observation was conducted without air exposure.

Fabrication and evaluation of the all-solid-state LIBs

All-solid-state LIBs were fabricated using $2.2\text{LiOH}\cdot\text{Li}_2\text{SO}_4$ with 5 mol% Li_3BO_3 as the solid electrolyte. The all-solid-state cells were fabricated and a series of battery tests were conducted in a dry room (dew point: $-40\text{ }^\circ\text{C}$). Graphite and $\text{Li}(\text{Ni}_{0.3}\text{Co}_{0.6}\text{Mn}_{0.1})\text{O}_2$ (hereafter, NCM) were used as the anode and cathode active materials, respectively [20]. To ensure electronic conduction in the cathode and anode layers, vapor-grown carbon fiber (VGCF, Showa Denko) was mixed at 2 vol%. NCM (or graphite), solid electrolyte,

and VGCF were weighed at 40:60:2 in a volume ratio, and then these were ground in a mortar. A total of 75 mg of $2.2\text{LiOH}\cdot\text{Li}_2\text{SO}_4$ with 5 mol% Li_3BO_3 powder was pressed at approximately 150 MPa for 1 min in a polyether ether ketone (PEEK) cylinder (inner diameter of 10 mm). The thickness of the solid electrolyte pellet was *ca.* 0.5 mm, which was attached and fixed inside the PEEK cylinder after pressing. The cathode (31 mg) and anode composites (33 mg) were mounted on each side of the preliminary pressed solid electrolyte. The anode/solid electrolyte/cathode pellet was hot-pressed at 150 MPa and maintained at 250 °C for 1 h. After the hot-pressing, the cell was loaded under 150 MPa by screwing, and the charge–discharge measurements were performed at 150 °C. In this study, 1 C was defined as 160 mA/g, and the net loading amount of NCM was approximately 18.4 mg. The details of the measurement conditions will be provided in the “Results and discussions” parts. To investigate the electrochemical stability of $2.2\text{LiOH}\cdot\text{Li}_2\text{SO}_4$ with 5 mol% Li_3BO_3 , cyclic voltammetry (CV) measurement was performed at 150 °C using Biologic, VMP3. The solid electrolyte was pressed at 150 MPa in a PEEK cylinder, and Li foil was fixed to one side of the pellet. Stainless steel (S.S.) disk was set on the other side of the solid electrolyte, which served as the working electrode. Finally, the Li/S.S. cell was pressed at 150 MPa.

Results and discussions

Materials characterization

Figure 1 shows XRD patterns of the reported stoichiometric compound, $3\text{LiOH}\cdot\text{Li}_2\text{SO}_4$ (Li_2SO_4 : 25 mol%) [14] and starting materials. Diffraction patterns of $3\text{LiOH}\cdot\text{Li}_2\text{SO}_4$ were identified with the PDF card number #032–0598 [13]. A subtle amount of LiOH was detected (marked as black circles in the figure), indicating that the reported $3\text{LiOH}\cdot\text{Li}_2\text{SO}_4$ is not the stoichiometric composition, and the single phase can be obtained for Li_2SO_4 -rich concentration. The variations of the crystalline phase with LiOH/ Li_2SO_4 ratio were investigated. For a sequence of samples, 5 mol% of Li_3BO_3 was mixed. As shown in Fig. 2, LiOH peaks were still observed for Li_3BO_3 -mixed $3\text{LiOH}\cdot\text{Li}_2\text{SO}_4$, indicating that the segregated LiOH does not react with Li_3BO_3 , and the strict composition of the line compound in LiOH- Li_2SO_4 system is deviated from 3:1. By increasing the prepared concentration of LiOH, the segregation of LiOH was minimized for $2.2\text{LiOH}\cdot\text{Li}_2\text{SO}_4$ (Li_2SO_4 : 31.3 mol%). Further increase of Li_2SO_4 resulted in the segregation of Li_2SO_4 (red circles). Diffraction peaks of Li_3BO_3 were not observed for the whole composition, which might be due to the small mixing amount of Li_3BO_3 . For $3\text{LiOH}\cdot\text{Li}_2\text{SO}_4$ with higher Li_3BO_3 concentration, the diffraction peaks of segregated Li_3BO_3 were observed while

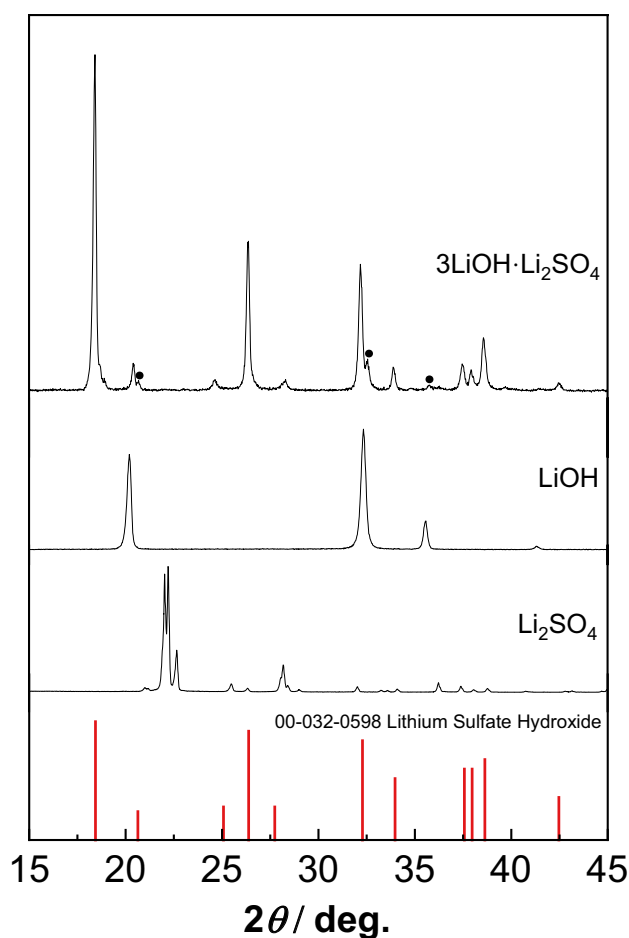


Fig. 1 XRD patterns of $3\text{LiOH}\cdot\text{Li}_2\text{SO}_4$ fabricated by melting at 430 °C. As a comparison, the simulated diffraction peak position (PDF#032–0598) and XRD patterns of starting materials are also presented at the bottom. The unreacted LiOH peaks are marked by black circles

the peak shift of $3\text{LiOH}\cdot\text{Li}_2\text{SO}_4$ was not clearly conformed (Fig. S1 in supplementary information). Hence, the formation of the solid solution with $3\text{LiOH}\cdot\text{Li}_2\text{SO}_4$, e.g., the substitution of SO_4^{2-} with BO_3^{3-} , is not likely. It is possible that Li_3BO_3 is mixing in an amorphous state in LiOH- Li_2SO_4 with 5 mol% Li_3BO_3 .

Electrical conductivities

Figure 3a shows the Arrhenius plot of the conductivities of LiOH- Li_2SO_4 with/without Li_3BO_3 . For $3\text{LiOH}\cdot\text{Li}_2\text{SO}_4$, which has been considered the stoichiometric composition, the conductivity was 4.2×10^{-7} S/cm at 23 °C which was slightly increased to 5.6×10^{-7} S/cm at 25 °C by Li_3BO_3 mixing. As shown in Fig. 3b, the conductivity maximum was observed when 5 mol% of Li_3BO_3 was added. Further increase of Li_3BO_3 fraction resulted in the decrease in the conductivity, which

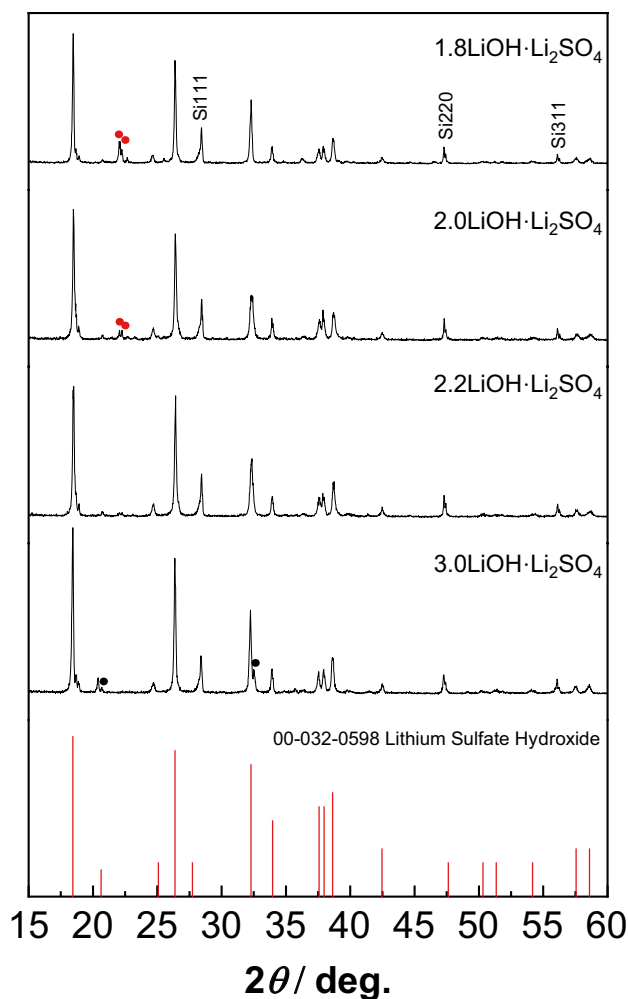


Fig. 2 XRD patterns of LiOH-Li₂SO₄ systems with four different LiOH/Li₂SO₄ compositions. 5 mol% of Li₃BO₃ was mixed for all samples. The diffraction peaks for segregated LiOH and Li₂SO₄ were denoted by black and red circles, respectively

can be due to the segregation of Li₃BO₃ (Fig. S1 in supplementary information). Although the detailed mechanism of the conductivity increase by Li₃BO₃ mixing was not clarified, a subtle amount of conductive phase such as 9Li₃BO₃·Li₂SO₄ might form at the interphase of the grain [21]. The conductivity was further enhanced by controlling the LiOH/Li₂SO₄ ratio. The conductivity of 2.2LiOH·Li₂SO₄ with 5 mol% of Li₃BO₃ was increased to 1.9×10^{-6} S/cm at 25 °C, which would be due to the decrease of the segregated LiOH (Fig. 1). This value is almost comparable to that of Li₂OHBr, which is known as the flexible solid electrolyte [9]. It is concluded that the conductivity of the LiOH-Li₂SO₄ system was optimized by controlling the LiOH/Li₂SO₄ ratio and Li₃BO₃ fraction. Hereafter, 2.2LiOH·Li₂SO₄ with 5 mol% of Li₃BO₃ will be denoted as LHS, and the battery tests and CV measurement are conducted for this composition.

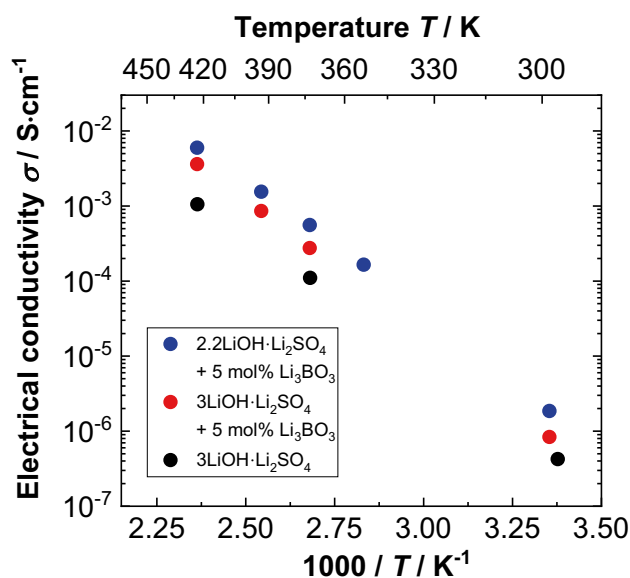


Fig. 3 Arrhenius plots of the conductivity of LiOH-Li₂SO₄. Activation energies for ion conduction are calculated as 0.70 eV, 0.76 eV, and 0.74 eV for 3LiOH·Li₂SO₄, 3LiOH·Li₂SO₄ with 5 mol% of Li₃BO₃ and 2.2LiOH·Li₂SO₄ with 5 mol% of Li₃BO₃, respectively

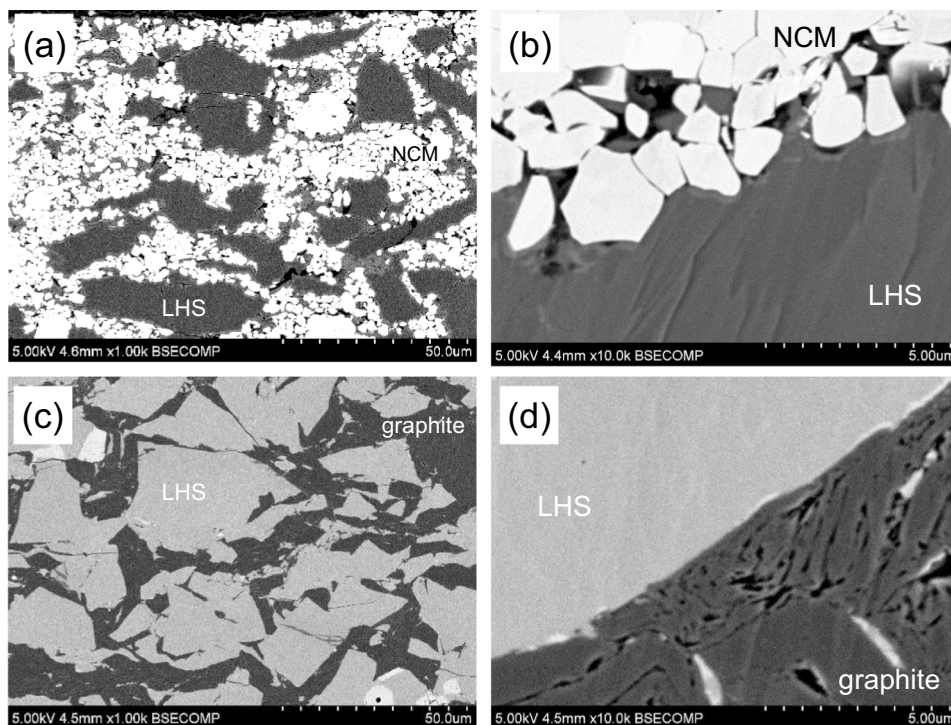
Microstructure of the battery

LHS was prepared by melting at 430 °C, indicating the all-solid-state battery can be constructed without high-temperature sintering. Hence, the batteries were fabricated by pressing under 150 MPa at 250 °C. Figure 4 shows backscattering electron images of the cross-section of the graphite/LHS/NCM cell. The bright contrast regions in Fig. 4a and b indicate the presence of NCM. In Fig. 4c and d, the dark contrast regions represent the graphite considering the difference in the atomic weight of graphite and LHS. LHS was infiltrated among the particles of active materials and formed intimate contacts. Note that these dense morphologies were constructed without high-temperature sintering, which is the great advantage for the practical application of the battery. As shown in Fig. S2 in supplementary information, LHS was not reacted with graphite and NCM at 250 °C, indicating the impurity phase is not present at the interphase after hot pressing.

Battery tests

Although the conductivity of the LiOH-Li₂SO₄ system was optimized and the dense interphases with the active materials were constructed, the conductivity at room temperature was not always sufficient for the high-rate charge–discharge cycling. Hence, the battery tests were conducted at 150 °C where the conductivity reached 6.0×10^{-3} S/cm. Figure 5 shows the results of the charge–discharge measurement of graphite/LHS/NCM cell at 150 °C. The cell was initially

Fig. 4 SEM images of the cross-section of **a, b** NCM/LHS and **c, d** graphite/LHS interphase after hot-pressing

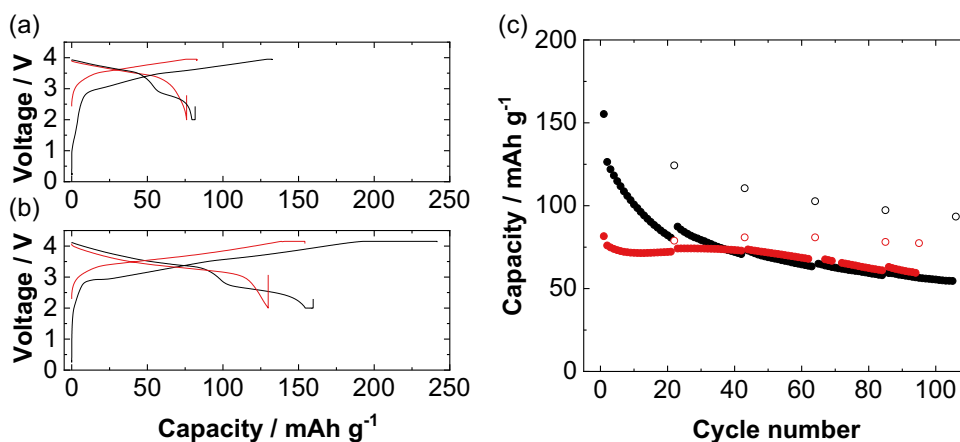


charged and discharged under 0.1 C (constant current mode) and maintained at the cutoff voltage until the current decayed to 0.01 C (constant voltage mode). At the second charging, the rate was increased to 1 C, and the termination current under the constant voltage mode was set as 0.1 C. The second discharging was conducted at 1 C without constant voltage discharging. As shown in Fig. 5a, first, the cell was charged to 3.95 V. At the initial charging, a charging capacity of 133 mAh/g was obtained. For the subsequent discharging, the capacity was decreased to 82 mAh/g. In addition to the discharge plateau of NCM, the voltage step was observed below 2.9 V. For the subsequent cycle, the charging capacity was 83 mAh/g which is almost the same as that of initial discharging. The voltage step observed at the initial

discharging was not observed for the second cycle. Figure 5b shows the charge–discharge curves in which the cutoff voltage was set as 4.15 V. The initial charging capacity was 242 mAh/g which is far exceeding the charging capacity of NCM under the cutoff voltage of 4.6 V [20], suggesting the parasitic oxidation (reduction) reaction at the cathode (anode) interphase. The subsequent discharge capacity was 160 mAh/g. The voltage step at 2.9 V was also observed at initial discharging, which disappeared at the second cycle.

The continuous charge–discharge cycling was performed for the 21st cycles under the same condition as the second cycle. After the 22nd cycle, the charge–discharge rate was decreased to 0.1 C while the constant voltage mode was the

Fig. 5 Charge–discharge curves of graphite/LHS/NCM cells with the upper cutoff voltage of **a** 3.95 V and **b** 4.15 V. The measurement was performed at 150 °C. Black and red lines represent the results for the first and second cycles, respectively. **c** Discharging capacities along with cycles. Red and black symbols represent the results under the upper voltage of 3.95 V and 4.15 V, respectively



same as those of the initial cycle. To confirm the capacity under a slow rate, the charge–discharge was performed under 0.01 C for each 20 cycles, whose results are plotted as white circles in Fig. 5c. The capacities were dropped for 20 cycles and gradually decreased for the subsequent cycles when the cutoff of the charging voltage was set as 4.15 V. These behaviors were almost the same under the slow rate charge–discharge. On the other hand, the overall capacities were decreased to ~ 70 mAh/g by lowering the cutoff voltage to 3.95 V while the drastic capacity fading was not observed. Discharge capacities of 80 mAh/g were obtained under 0.01 C. The charge–discharge properties of the graphite/LHS/NCM cell were largely influenced by the cutoff voltage at charging. The electrochemical stability of LHS and the microstructure of the interphase with NCM and graphite along the cycle were investigated.

Figure 6 represents the CV curves of the Li/S.S. cell with LHS electrolyte. First, the voltage was swept from OCP (~ 2.7 V) to 1.2 V. Subsequently, the cell was polarized to 4.2 V and finally returned to the initial voltage. Two reduction current peaks were observed at 2.3 V and 1.6 V, indicating the reductive decomposition of LHS. Above 3.6 V, the oxidation current was observed, which was largely increased above 3.8 V. To specifically investigate the electrochemical stability at each voltage region, the voltage was separately swept between OCP/1.2 and OCP/4.2 V using the different cells. At high voltage, the oxidation current was slightly reduced with cycles; however, the oxidation of the solid electrolyte perpetually proceeded. On the other hand, the reductive decomposition was suppressed along with the cycle, indicating the passivation behavior at the anode interphase. These CV results

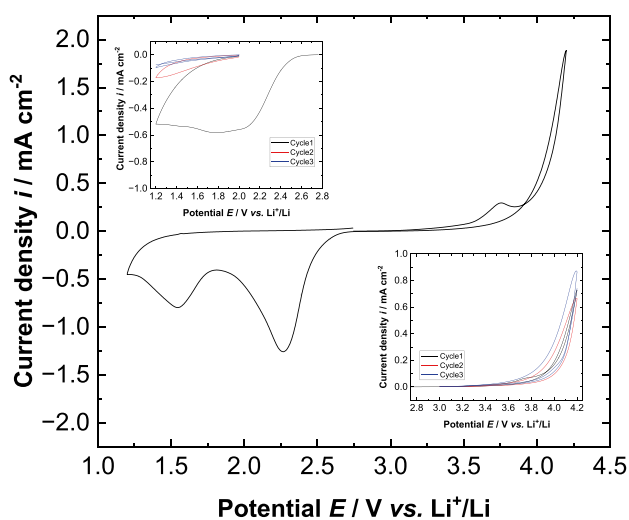


Fig. 6 CV curves of Li/S.S. cell at 150 °C. The insets in the left and right side of the figure show the results solely swept between OCP/1.2 V and OCP/4.2 V, respectively

are consistent with the variation of the microstructure of the electrode interphases. Figure 7a–c shows SEM images of the interphase of LHS/NCM after charging at the different SOC. The reaction layer was observed in a different contrast at the interphase, which grew with increasing the cutoff voltage. This interphase layer included significant amounts of pores, which perhaps represents the gas release during charging. On the other hand, the microstructure of the graphite interphase was not largely changed even after cycling 80 times (Fig. 7d), indicating that the reduction reaction at the graphite interphase did not continuously proceed. The detailed reaction mechanism has not been identified. Considering the chemical composition of the solid electrolyte ($2.2\text{LiOH}\cdot\text{Li}_2\text{SO}_4$ with 5 mol% of Li_3BO_3), the possible reduction products are Li_2O and Li_2S . The decomposition of Li_3BO_3 can result in the formation of Li_xB [22], which is electronic conductive [23]. However, from the past report by Ding et al., the reduction of BO_3^{3-} ions was not clearly confirmed at the interphase of Li/ Li_3BO_3 [24]. Considering the concentration of Li_3BO_3 in LHS (5 mol%), it can be said that the decomposition of Li_3BO_3 is less dominant compared with that of $2.2\text{LiOH}\cdot\text{Li}_2\text{SO}_4$. The predicted reduction products of $2.2\text{LiOH}\cdot\text{Li}_2\text{SO}_4$, Li_2O , and Li_2S , are electron insulators. Hence, the continuous electron path in the decomposition layer would be interrupted once the interphase is covered by the decomposition products. The interruption of electron supply from the current collector hinders the further decomposition of LHS, which might be the passivation mechanism at the anode interphase. The situation can be similar for the cathode interphase. The possible oxidation products are O_2 and S [25]. It seems there are no metallic compounds, while the decomposition layer was increased during charging (Fig. 7). The gas released during charging would form the pores at the interphase. After the gas release, the remained interphase would be unreacted LHS and maintain the interphase in an initial state. In the present study, the cell was pressed at 150 MPa during charge–discharge measurement. Hence, it is speculated that the pores formed by the gas release can be pressed by cell loading and disappear, which results in the recovery of the contact of unreacted LHS with NCM. This repetition of the pore formation and the recovery of the “fresh” contact by pressing at the interphase can result in the continuous oxidation of the solid electrolyte. However, when the cell was cycled without loading, the capacities were decreased, and cycle stability was degraded (Fig. S3 in supplementary information). Because of the volume change of graphite anode during Li intercalation/deintercalation, a certain degree of the cell loading might be needed to maintain the intimate contact between LHS and graphite for the stable performance, which hinders the specific investigation of the effect of the cell loading on the side reaction at cathode interphase. Because LHS includes

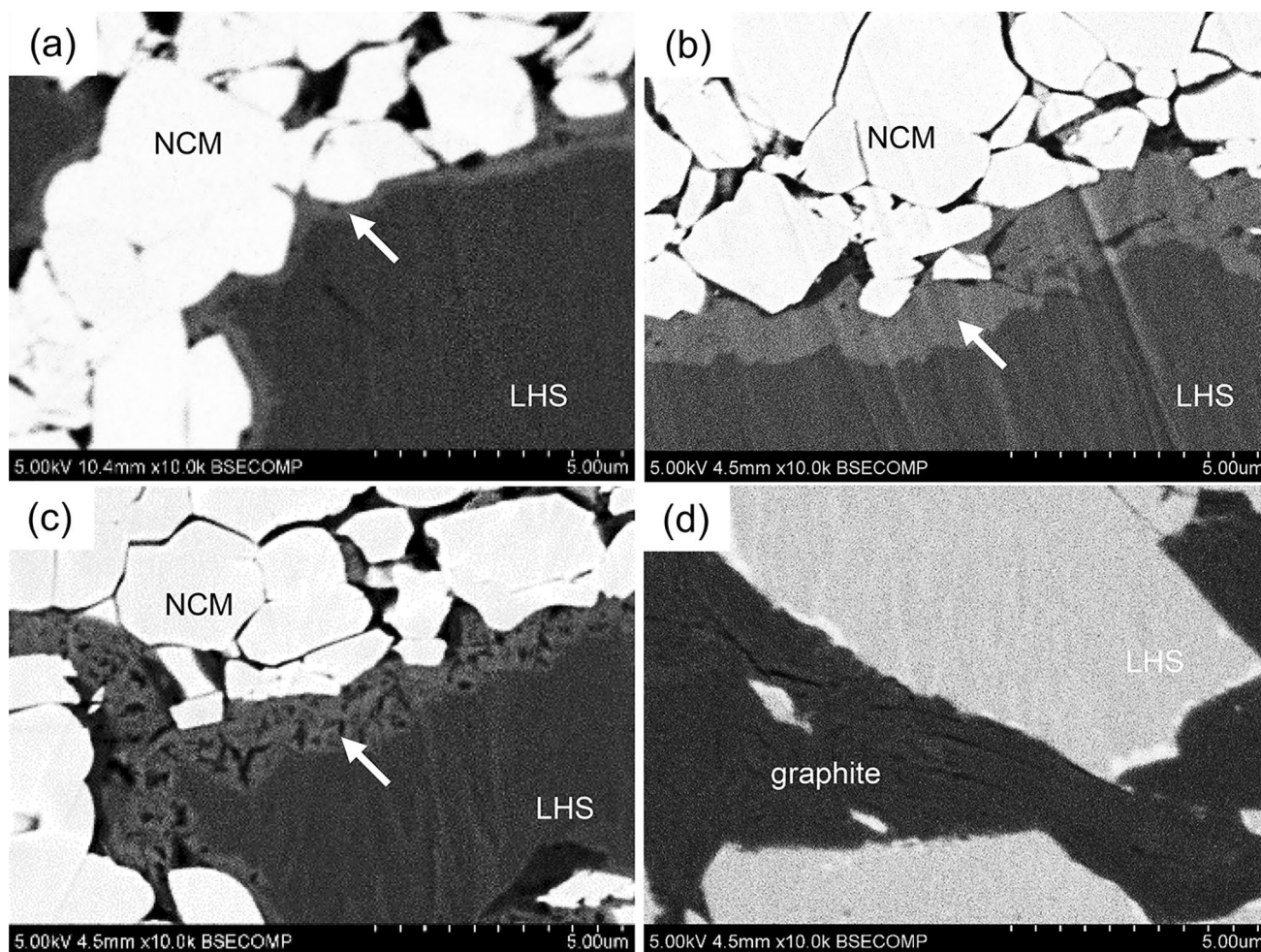


Fig. 7 SEM images of the cross-section of NCM/LHS interphase after initial charging at **a** 3.75 V, **b** 3.95 V and **c** 4.15 V. **d** SEM image of graphite/LHS interphase after 80 cycles. The decomposition layers at the interphase were presented by white arrows

OH^- ions, the presence of H_2O can also be predicted as the oxidation products, which would be further oxidized to O_2 and H^+ at high voltage [26]. H^+ insertion into NCM might also affect the charge–discharge performances [27]. The charge–discharge performances were stable by restricting the charging voltage at 3.95 V, indicating that stable cycling is expected using the moderately high voltage cathodes such as LiFePO_4 and S. It should be emphasized that the batteries were fabricated in a dry room, and the intimate electrode contact was constructed by hot-pressing. The stable cycle performances and high powder pressing ability of LHS in conjunction with the high tolerance for the oxygen atmosphere indicate the possibility that LHS is not only used as molten flux for the preparation of single crystals but also for the soft solid electrolyte for all-solid-state LIBs. The flexible nature of LHS can also be used as the sintering additive of the oxide solid electrolyte [28, 29].

Conclusions

In this study, $\text{LiOH}\cdot\text{Li}_2\text{SO}_4$ systems were fabricated by melting, and the line compound was determined. The compositional dependence of the ionic conductivity of $\text{LiOH}\cdot\text{Li}_2\text{SO}_4$ was investigated. For $3\text{LiOH}\cdot\text{Li}_2\text{SO}_4$, which is the previously known composition, unreacted LiOH was included. The single phase was obtained for Li_2SO_4 -rich composition, $2.2\text{LiOH}\cdot\text{Li}_2\text{SO}_4$. The conductivity was optimized by controlling $\text{LiOH}/\text{Li}_2\text{SO}_4$ ratio and Li_3BO_3 concentration. The maximum conductivity was 1.9×10^{-6} and 6.0×10^{-3} S/cm at 25 and 150 °C, respectively, for $2.2\text{LiOH}\cdot\text{Li}_2\text{SO}_4$ with 5 mol% of Li_3BO_3 . The dense contacts of NCM/LHS and graphite/LHS were formed by hot pressing at 250 °C under 150 MPa. The all-solid-state cell was fabricated in a dry room where the dew point was maintained at -40 °C, indicating that LHS is stable under an oxygen atmosphere.

The charge–discharge performances of the graphite/LHS/NCM cell were stable; the discharge capacity of 80 mAh/g was maintained under 0.01 C for 100 cycles when the SOC of NCM was restricted to 3.95 V. Although the capacity was decreased at the initial 20 cycles when the cell was charged to 4.15 V (corresponding to the 100% SOC of NCM), the subsequent cycle was stable without drastic capacity fading. The reductive decomposition of LHS was observed at 2.3 and 1.6 V in the CV curves. These reduction currents were decreased with cycling. On the other hand, the oxidation current was observed above 3.6 V, indicating LHS underwent the oxidative decomposition. This oxidation current was not decreased with the repetition of voltage cycling. The results of SEM observation also suggest that LHS is less tolerable under high voltage. The growth of the reaction layer at the NCM interphase was observed in the SEM image after charging. Such a reaction layer was not clearly confirmed at the graphite interphase. The anode interphase can be passivated possibly by forming insulating compounds, Li_2O and Li_2S .

Supplementary Information The online version contains supplementary material available at <https://doi.org/10.1007/s10008-023-05656-x>.

Acknowledgements This work was supported by the NGK Environment Innovation Laboratory.

References

- Pan H, Cheng Z, He P, Zhou H (2020) A review of solid-state lithium–sulfur battery: ion transport and polysulfide chemistry. *Energy Fuels* 34:11942–11961. <https://doi.org/10.1021/acs.energyfuels.0c02647>
- Hikima K, Suzuki K, Taminato S, Hirayama M, Yasuno S, Kanno R (2019) Thin film all-solid-state battery using Li_2MnO_3 epitaxial film electrode. *Chem Lett* 48:192–195. <https://doi.org/10.1246/cl.180773>
- Kobayashi Y, Takeuchi T, Tabuchi M, Kageyama H (1999) Densification of $\text{LiTi}_2(\text{PO}_4)_3$ -based solid electrolytes by spark-plasma-sintering. *J Power Sources* 81–82:853–858
- Sakuda A, Hayashi A, Tatsumisago M (2013) Sulfide solid electrolyte with favorable mechanical property for all-solid-state lithium battery. *Sci Rep* 3:2261. <https://doi.org/10.1038/srep02261>
- Unemoto A et al (2014) Development of bulk-type all-solid-state lithium–sulfur battery using LiBH_4 electrolyte. *Appl Phys Lett* 105:083901. <https://doi.org/10.1063/1.4893666>
- Unemoto A, Yoshida K, Ikeshoji T, Orimo S-I (2016) Bulk-type all-solid-state lithium batteries using complex hydrides containing cluster-anions. *Mater Trans* 57:1639–1644. <https://doi.org/10.2320/matertrans.MAW201601>
- Yoshikawa K, Yamamoto T, Sugumar MK, Motoyama M, Iriyama Y (2021) Room temperature operation and high cycle stability of an all-solid-state lithium battery fabricated by cold pressing using soft Li_2OHBr solid electrolyte. *Energy Fuels* 35:12581–12587. <https://doi.org/10.1021/acs.energyfuels.1c01190>
- Unemoto A et al (2015) Stable interface formation between TiS_2 and LiBH_4 in bulk-type all-solid-state lithium batteries. *Chem Mater* 27:5407–5416. <https://doi.org/10.1021/acs.chemmater.5b02110>
- Sugumar MK, Yamamoto T, Motoyama M, Iriyama Y (2020) Room temperature synthesis of anti-perovskite structured Li_2OHBr . *Solid State Ionics* 349:115298. <https://doi.org/10.1016/j.ssi.2020.115298>
- Gao L, Zhao R, Han S, Li S, Zou R, Zhao Y (2021) Antiperovskite ionic conductor Layer for stabilizing the interface of NASICON solid electrolyte against Li metal in all-solid-state batteries. *Batteries Supercaps* 4:1491–1498. <https://doi.org/10.1002/batt.202100123>
- Tatsumisago M, Takano R, Tadanaga K, Hayashi A (2014) Preparation of Li_3BO_3 – Li_2SO_4 glass–ceramic electrolytes for all-oxide lithium batteries. *J Power Sources* 270:603–607. <https://doi.org/10.1016/j.jpowsour.2014.07.061>
- Nagao K, Nose M, Kato A, Sakuda A, Hayashi A, Tatsumisago M (2017) Preparation and characterization of glass solid electrolytes in the pseudoternary system Li_3BO_3 – Li_2SO_4 – Li_2CO_3 . *Solid State Ionics* 308:68–76. <https://doi.org/10.1016/j.ssi.2017.05.009>
- Biefeld RM, Johnson RT, J. (1979) The effects of Li_2SO_4 addition, moisture, and LiOH on the ionic conductivity of Li_5AlO_4 . *J Solid State Chem* 29:393–399
- Deshpande VK, Raghuvanshi FC, Singh K (1986) Electrical conductivity of the Li_2SO_4 –LiOH system. *Solid State Ionics* 18&19:378–381
- Singh K, Raghuvanshi FC (1988) Li_2SO_4 –LiOH eutectic system, a promising solid electrolyte. *Solid State Ionics* 28–30:267–270
- Dai P, Kong X, Yang H, Li J, Zeng J, Zhao J (2022) Single-crystal Ni-Rich layered $\text{LiNi}_{0.9}\text{Mn}_{0.1}\text{O}_2$ enables superior performance of Co-free cathodes for lithium-ion batteries. *ACS Sustainable Chemistry & Engineering* 10:4381–4390. <https://doi.org/10.1021/acssuschemeng.1c06704>
- Li S et al (2022) Thermal-healing of lattice defects for high-energy single-crystalline battery cathodes. *Nat Commun* 13:704. <https://doi.org/10.1038/s41467-022-28325-5>
- Qian G et al (2022) Value-creating upcycling of retired electric vehicle battery cathodes. *Cell Reports Physical Science* 3:100741. <https://doi.org/10.1016/j.xcrp.2022.100741>
- Takamori S, Doi T, Inaba M (2023) Aluminum doping effects on large $\text{LiNi}_{0.8}\text{Co}_{0.1}\text{Mn}_{0.1}\text{O}_2$ single crystal particles prepared in a molten LiOH – Li_2SO_4 flux. *J Electrochem Soc* 170:020532. <https://doi.org/10.1149/1945-7111/acbc51>
- Strauss F et al (2020) Rational Design of Quasi-Zero-Strain NCM cathode materials for minimizing volume change effects in all-solid-state batteries. *ACS Materials Letters* 2:84–88. <https://doi.org/10.1021/acsmaterialslett.9b00441>
- Tatsumisago M et al (2017) Electrical and mechanical properties of glass and glass-ceramic electrolytes in the system Li_3BO_3 – Li_2SO_4 . *J Ceram Soc Jpn* 125:433–437. <https://doi.org/10.2109/jcersj2.17026>
- Hensley DA, Garofalini SH (1994) XPS investigation of lithium borate glass and the Li – LiBO_2 interface. *Appl Surf Sci* 81:331–339
- Dudakov IV, Solntsev KA (2009) Theoretical prediction of the new high-density lithium boride LiB_{11} with polymorphism and pseudoplasticity. *Russ J Inorg Chem* 54:1261–1272. <https://doi.org/10.1134/s0036023609080142>
- Ding X, Xin Y, Wang Y, Wang M, Song T, Gao H (2023) Artificial solid electrolyte interphase engineering toward dendrite-free lithium anodes. *ACS Sustainable Chemistry & Engineering* 11:6879–6889. <https://doi.org/10.1021/acssuschemeng.2c06146>
- Zhu Y, He X, Mo Y (2015) Origin of outstanding stability in the lithium solid electrolyte materials: insights from thermodynamic analyses based on first-principles calculations. *ACS Appl Mater Interfaces* 7:23685–23693. <https://doi.org/10.1021/acsami.5b07517>
- Guo L et al (2021) The electrolysis of anti-perovskite Li_2OHCl for prelithiation of high-energy-density batteries. *Angew Chem Int Ed Engl* 60:13013–13020. <https://doi.org/10.1002/anie.202102605>
- Posada-Pérez S, Rignanes G-M, Hautier G (2021) Influence of stacking on H^+ intercalation in layered ACoO_2 ($A = \text{Li}, \text{Na}$) cathode materials and implications for aqueous Li-Ion batteries: a

- first-principles investigation. *Chem Mater* 33:6942–6954. <https://doi.org/10.1021/acs.chemmater.1c01887>
28. Reddy IN et al (2020) A systematic study of annealing environment and Al dopant effect on NASICON-type $\text{LiZr}_2(\text{PO}_4)_3$ solid electrolyte. *Ionics* 26:4287–4298. <https://doi.org/10.1007/s11581-020-03622-5>
29. Akkinepally B et al (2022) Dopant effect on Li^+ ion transport in NASICON-type solid electrolyte: insights from molecular dynamics simulations and experiments. *Ceram Int* 48(9):12142–12151. <https://doi.org/10.1016/j.ceramint.2022.01.075>

Publisher's Note Springer Nature remains neutral with regard to jurisdictional claims in published maps and institutional affiliations.

Springer Nature or its licensor (e.g. a society or other partner) holds exclusive rights to this article under a publishing agreement with the author(s) or other rightsholder(s); author self-archiving of the accepted manuscript version of this article is solely governed by the terms of such publishing agreement and applicable law.